

# Sensitivity Decouple Learning for Image Compression Artifacts Reduction

Li Ma, Yifan Zhao, Peixi Peng, and Yonghong Tian, *Fellow, IEEE*

**Abstract**—With the benefit of deep learning techniques, recent researches have made significant progress in image compression artifacts reduction. Despite their improved performances, prevailing methods only focus on learning a mapping from the compressed image to the original one but ignore the intrinsic attributes of the given compressed images, which greatly harms the performance of downstream parsing tasks. Different from these methods, we propose to decouple the intrinsic attributes into two complementary features for artifacts reduction, *i.e.*, the compression-insensitive features to regularize the high-level semantic representations during training and the compression-sensitive features to be aware of the compression degree. To achieve this, we first employ adversarial training to regularize the compressed and original encoded features for retaining high-level semantics, and we then develop the compression quality-aware feature encoder for compression-sensitive features. Based on these dual complementary features, we propose a Dual Awareness Guidance Network (DAGN) to utilize these awareness features as transformation guidance during the decoding phase. In our proposed DAGN, we develop a cross-feature fusion module to maintain the consistency of compression-insensitive features by fusing compression-insensitive features into the artifacts reduction baseline. Our method achieves an average 2.06 dB PSNR gains on BSD500, outperforming state-of-the-art methods, and only requires 29.7 ms to process one image on BSD500. Besides, the experimental results on LIVE1 and LIU4K also demonstrate the efficiency, effectiveness, and superiority of the proposed method in terms of quantitative metrics, visual quality, and downstream machine vision tasks.

**Index Terms**—Compression artifacts reduction, intrinsic attributes, Dual awareness guidance network, Compression-sensitive features, Compression-insensitive features.

## I. INTRODUCTION

**T**HE explosive growth of multimedia data, especially images and videos, brings significant challenges to bandwidth and resources. Thus, lossy compression methods have become widely applied techniques to reduce information redundancy and save storage space and transmission time. However, due to the inevitable information loss in these compression operations, complex artifacts, such as blocking and ringing artifacts, are usually introduced into compressed images and videos. These artifacts reduce the visual quality

Li Ma and Yifan Zhao contributed equally. Corresponding authors: Peixi Peng and Yonghong Tian.

Li Ma is with the Huawei Technologies Company, Ltd, Shenzhen, 518129, China, (e-mail: mali93@huawei.com).

Yifan Zhao is with the State Key Laboratory of Virtual Reality Technology and Systems, School of Computer Science and Engineering, Beihang University, Beijing, 100191, China. (e-mail: zhaoyf@buaa.edu.cn)

Peixi Peng, and Yonghong Tian are with the School of Electronics and Computer Engineering and the School of Computer Science, Peking University, Beijing, 100871, China, and the PengCheng Laboratory, Shenzhen, 518055, China, (e-mail: ppxpeng@pku.edu.cn; yhtian@pku.edu.cn).

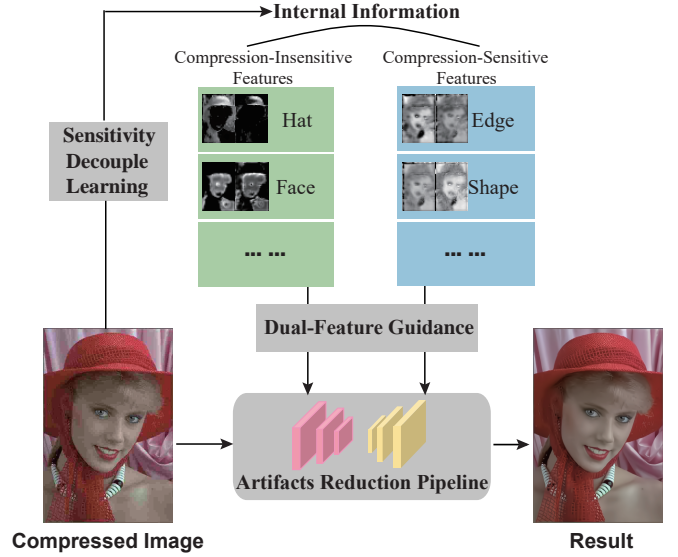


Fig. 1. The motivation of the proposed sensitivity decouple learning, which explicitly mines the intrinsic attributes from the given compressed image. The proposed method decouples the intrinsic image attributes into compression-insensitive features for high-level semantics (*e.g.*, hat and face) and compression-sensitive features for low-level cues (*e.g.*, edge and shape).

and the performance of downstream parsing tasks, especially at high compression ratios.

Compression artifacts reduction tasks aim at reducing the artifacts caused by lossy compression, *i.e.*, predicting original (uncompressed) images or videos from compressed ones. Prevailing compression artifacts reduction methods could fall into three classes: filter-based methods [1]–[3], prior-based methods [4]–[11], and learning-based methods [12]–[57]. The pioneer works [1]–[3] design handcrafted filters to reduce compression artifacts, which results in inferior results when processing images or videos with complicated patterns. Since compression artifacts reduction could be regarded as ill-posed inverse problems, prior knowledge plays an essential role in the process. Several works propose to design effective priors to constrain the solution space [4]–[11]. Despite the higher performance they achieved, the representation abilities of handcrafted priors are still limited and usually fixed under different complex scenarios.

Inspired by the advances in deep learning techniques, recent research efforts [12]–[57] propose to learn the inverse mapping of compressed images to original ones by deep neural networks. Despite their improved performances, these methods consider this process as an *implicit* end-to-end learning process

while neglecting the intrinsic attributes during compression, leading to unbalanced views of features when restoring images. For example, an artifacts reduction network that is well-trained on human face images shows an unsatisfactory performance when processing natural scene images. Hence, in this paper, we try to answer the following question: How to *explicitly* model the intrinsic attributes during the compression process and thus guide the learning of artifacts reduction?

To address this issue, we make an insightful attempt to decouple the compression intrinsic attributes into two complementary aspects: 1) compression-insensitive features: the compressed images and original images should share the same semantic representations, *e.g.*, both belonging to the same *person* class in Fig. 1. We thus resort to feature discriminator on high-level semantics by training a compression-insensitive auto-encoder beyond the basic restoration. In this manner, the semantic representations of compressed images and original ones could play similar effects when adapting to downstream high-level vision tasks, spanning over semantic segmentation, object detection, and recognition. 2) compression-sensitive features: The local details, including blurriness and boundary sharpness, are easy to lose during compression. As it is hard to definite them using specific measurements, we thus propose to make the encoded features aware of quality factors, which reflect the degree of compression and are available in the compressed files. Based on these two decoupled aspects of features, our key idea is to utilize these features as learning guidance to adapt the decoded feature to various scenarios. Thereby, we introduce a new compression artifacts reduction framework, namely Dual Awareness Guidance Network (DAGN), which benefited from the successful decoupling of the semantic compression-insensitivity and low-level compression-sensitivity. Beyond the dual-awareness guidance, we also propose a cross-feature fusion module to incorporate the multi-scale semantic information from the compression-insensitive encoders. With the joint learning of the decoupling learning and dual awareness guidance, our proposed Dual Awareness Guidance Network is able to understand the low-level cues while also maintaining high-level semantic information during the image restoration process. To verify these contributions, we conduct experiments by two lines of results: 1) for visual quality, the proposed DAGN achieves superior performance against state-of-the-art methods on quantitative metrics, including PSNR and SSIM; 2) for downstream high-level vision tasks, we provide qualitative and quantitative results on object detection and semantic segmentation tasks after our artifacts reduction.

Our major contributions are as follows:

- We revisit the compression process from a new perspective of decoupling learning and propose two compression awareness modules: the compression-insensitive modules for high-level semantics and the compression-sensitive module for compression details.
- We propose a Dual Awareness Guidance Network with a dual awareness guidance module to adapt the decoding process for various conditions and a cross-feature fusion module for multi-scale semantic enhancement.
- Extensive experiments are performed on synthetic and

real compressed image datasets to validate the effectiveness and superiority of DAGN. We demonstrate that DAGN achieves favorable performance against state-of-the-art methods in both visual quality measurements and vision parsing tasks.

The remainder of this paper is organized as follows. Section II reviews related works, and Section III describes the proposed Dual Awareness Guidance Network. Experiments and analyses of the proposed method are presented in Section IV. Section V finally concludes this paper.

## II. RELATED WORK

Compression artifacts belong to image-dependent noises, and researchers have proposed numerous methods to reduce these artifacts [6], [40], primarily *filtering-based methods*, *model-based methods*, and *learning-based methods*.

### A. Filtering-based methods

Early methods pay attention to filter design. Zhai *et al.* [1] construct a neighborhood related to the correlation in regions and utilize the filter in blocks. Yoo *et al.* [2] propose to apply group-based filters to edge blocks and their similar ones. Besides filtering in the pixel domain, Foi *et al.* [3] propose to conduct filtering in the frequency domain. Overall, these early methods usually have limited performance when meeting images or videos with complicated patterns due to the limited representation capabilities of handcrafted filters.

### B. Prior-based methods

Since artifacts reduction is ill-posed, it could be formulated as a maximum posterior problem, where prior knowledge could play an essential role in the process. Some priors come from the compression process, such as quantization steps, and transformation coefficients could be used to constrain the artifacts reduction results [4], [5]. Besides, researchers have utilized priors related to natural images, such as low rank [9], non-local self-similarity [10], representation [6]–[8], and graph [11], to reduce compression artifacts. However, these methods usually need iterative computations, which are significantly time-consuming.

### C. Learning-based methods

Learning-based methods aim to learn a mapping from compressed images to the original ones. Due to the powerful representation ability, deep neural networks have greatly improved compression artifacts reduction in recent years [12]–[57]. The first deep neural networks-based method [41] proposes a 4-layer network named ARCNN. Motivated by the success of ResNet [58] in image classification, deeper networks with residual learning are proposed for compression artifacts reduction, such as DnCNN [16], RNAN [15], and RDN [23]. Later, inspired by the superior performance of Transformer [59], researchers also introduce Transformer for compression artifacts reduction [45]–[48]. Based on the standard Transformer architecture, Chen *et al.* propose an image processing transformer for image restoration problems [45]. Liang *et al.* design

SwinIR based on the Swin Transformer, which achieves better performance with fewer parameters. Meanwhile, researchers propose to employ the generative adversarial network (GAN) [60] for compression artifacts reduction to recover visually satisfying results from compressed images [30]–[32].

Besides approaches in the pixel domain, researchers propose many dual-domain learning-based methods [25], [27]–[29], [31], [61], [62], which exploit the knowledge of the frequency domain to reduce the artifacts. Li *et al.* [35] propose a single network to process images compressed at all levels, which takes quantization steps and compressed images as input. To solve blind artifacts reduction where the quality factor (QF) is unavailable, Jiang *et al.* [13] and Kim *et al.* [36] estimate QF by a network and then utilize the estimated QF to guide artifacts reduction. Here, QF is an important index reflecting the compression degree of JPEG images, and a lower QF means less size is required, but more information is lost. Recently, some researchers endeavor to combine prior-based and learning-based methods for compression artifacts reduction, where deep neural networks are employed to learn priors and perform as regularizers under the alternative minimization framework [44], [49]–[57]. Dong *et al.* [50] adopt the half-quadratic splitting method to solve the minimization problem and designed a Denoising Prior Driven Deep Neural Network. Zhang *et al.* [49], [52] set up a benchmark deep prior by training a highly flexible and effective CNN denoiser. Jo *et al.* [51] analyze the prior by the notion of practical degrees of freedom to monitor the optimization progress. Fu *et al.* [54] utilize dictionary learning to model compression priors and design an iterative optimization algorithm using proximal operators. Subsequently, the priors used for this task are further differentiated. Fu *et al.* [53] propose two prior terms for the image content and gradient, respectively. The content-relevant prior is formulated as an image-to-image regressor to perform as a deblocker from the pixel level. The gradient-relevant prior serves as a classifier to distinguish whether the image is compressed from the semantic level. Zha *et al.* [44] propose a pair of triply complementary priors, namely, internal and external, shallow and deep, and non-local and local priors. They design a hybrid plug-and-play framework and a joint low-rank and deep image model based on the priors. Overall, These methods increase the interpretability of deep neural networks for compression artifacts reduction.

To summarize, learning-based approaches have significantly improved the performance of image compression artifacts reduction. However, the intrinsic attributes during the compression process are substantially neglected by prevailing methods. Hence, in this paper, we explore decoupling the compression image attributes from semantic-aware insensitive features and quality-aware sensitive features.

### III. APPROACH

#### A. Sensitivity Decouple Learning

We first set up the basic notations used in this paper. Let  $\mathbf{o}$  and  $\mathbf{c}$  denote the original image and its compressed version.  $\mathbf{A}_\mathbf{o}$  and  $\mathbf{A}_\mathbf{c}$  be the corresponding intrinsic attributes,

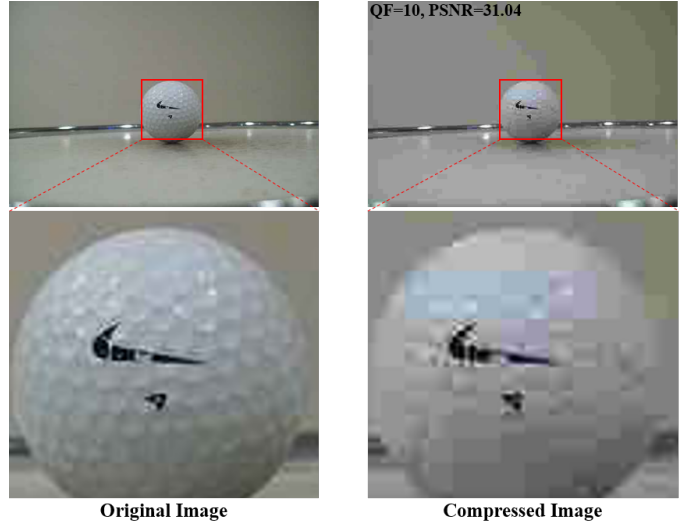


Fig. 2. An original image and its JPEG compressed version with QF = 10 that shows the relationship between the intrinsic attributes and compression. Some intrinsic attributes are changed by JPEG compression, such as *dimples*, while others are maintained, such as *sphere*.

respectively. Consider a given original image  $\mathbf{o}$ , and prevailing learning-based methods dedicate to learning a mapping function  $\mathcal{F}$  from  $\mathbf{c}$  to  $\mathbf{o}$ :

$$\min_{\theta_{\mathcal{F}}} \mathcal{L}(\mathcal{F}(\mathbf{c}; \theta_{\mathcal{F}}), \mathbf{o}), \quad (1)$$

where  $\mathcal{F}(\cdot; \theta_{\mathcal{F}})$  denotes the artifacts reduction network whose parameters are  $\theta_{\mathcal{F}}$ ;  $\mathcal{L}$  is the evaluation metric, usually mean absolute error or mean square error. This paper aims to obtain  $\mathbf{A}_\mathbf{c}$  from  $\mathbf{c}$  to promote the artifacts reduction process:

$$\min_{\theta_{\mathcal{F}}} \mathcal{L}(\mathcal{F}(\mathbf{c}; \theta_{\mathcal{F}} | \mathbf{A}_\mathbf{c}), \mathbf{o}). \quad (2)$$

During the compression process, it is known that some certain attributes in  $\mathbf{A}_\mathbf{c}$  are usually broken or degraded, while others are substantially retained. Therefore, we argue that these two components contain different cues: the unbroken part holds some high-level semantic information, while the broken part reflects the degree of compression/quality. In Fig. 2, we could obtain *sphere* and *block patterns on the surface* from the compressed image. Comparing the compressed image with the original one, we could observe that *sphere* is not broken by compression, while *block patterns on the surface* are broken during compression. In other words, we could obtain *sphere* and *dimples* from the original image. *sphere* exists in the compressed image, while *dimples* do not exist and are replaced by *block patterns on the surface*. Therefore, considering the maintenance during compression, the intrinsic attributes of compressed images can be divided into two complementary components, *i.e.*, compression-insensitive features  $\mathbf{F}_{cif}$  and compression-sensitive features  $\mathbf{F}_{csf}$ .  $\mathbf{F}_{cif}$  shares similar high-level semantic information with the original image, while  $\mathbf{F}_{csf}$  holds the information related to the low-level qualities, which are highly related to the Quality Factors (QF). To decouple these two features,  $\mathbf{F}_{cif}$  and  $\mathbf{F}_{csf}$  from  $\mathbf{c}$ , we employ a common approach that automatically learns features from

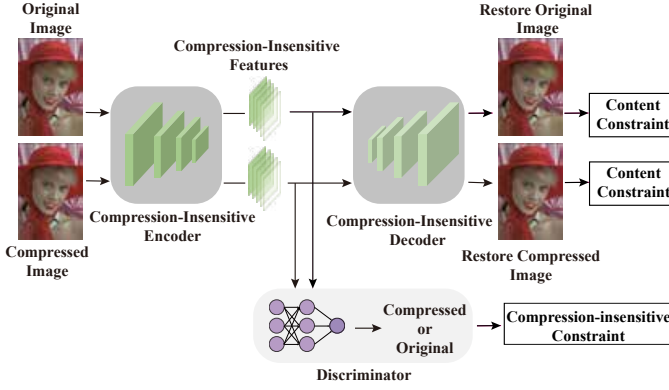


Fig. 3. The training of compression-insensitive auto-encoder. The discriminator takes the features learned by the compression-insensitive encoder as the input and generates the probability that the features are from original images. By training the auto-encoder to fool the differentiable discriminator network, we obtain the compression-insensitive encoder that could extract compression-insensitive features from images.

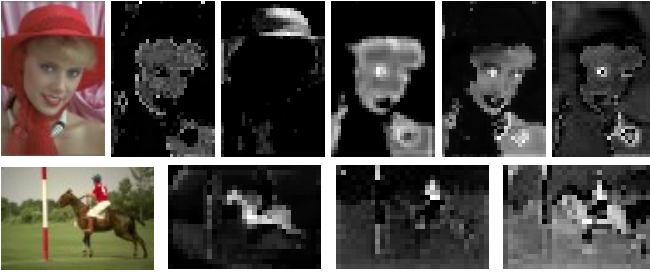


Fig. 4. Visualization of the compression-insensitive features learned from *womanhat* in LIVE1 and *206062* in BSD500.

unlabeled data, auto-encoders [63]–[67]. Bengio *et al.* [63] summarize the formulation of auto-encoders and discuss their connection to Restricted Boltzmann Machines. Ng *et al.* [64] impose a sparsity constraint on the hidden units of the auto-encoders and explore the structure in the data. Meng *et al.* [66] propose a relation auto-encoder that could extract high-level features based on both data itself and their relationships. Tschannen *et al.* [67] review representation learning with a focus on auto-encoder-based models, which could be referred to get a quick understanding of auto-encoder. We define them in a former way: one typical auto-encoder could be considered to include two modules: one encoder  $\mathcal{E}(\cdot; \theta_{\mathcal{E}})$  to embed the image into feature representations; and one decoder  $\mathcal{D}(\cdot; \theta_{\mathcal{D}})$  to reconstruct and estimate the uncompressed images from the representations, which could be denoted as  $\mathcal{D}(\mathcal{E}(\cdot; \theta_{\mathcal{E}}); \theta_{\mathcal{D}})$ .

1) *Compression-Insensitive Auto-Encoder*: Our key idea for constructing compression-insensitive features is to maintain the semantic consistency of original and compressed images through adversarial training. We denote the auto-encoder to extract compression-insensitive features as  $\mathcal{E}_{ci}(\cdot; \theta_{\mathcal{E}}^{ci})$  and  $\mathcal{D}_{ci}(\cdot; \theta_{\mathcal{D}}^{ci})$ . Specifically, the former is a modified ResNet-50 encoder whose average-pooling layers are removed, and the last stride 2 convolution is replaced with stride 1. The latter is a 15-layer fully convolutional decoder, consisting of 5 convolutional layers followed by alternating convolution and convolution transpose layers. For compression-insensitive

features, we employ a discriminator network  $\mathcal{J}(\cdot; \theta_{\mathcal{J}})$  which is a  $2048 \times 2048 \times 1$  MLP. In other words, if the high-level features of original images and compressed ones could not be distinguished, their features would be highly consistent.  $\mathcal{J}(\cdot; \theta_{\mathcal{J}})$  takes the features learned by  $\mathcal{E}_{ci}(\cdot; \theta_{\mathcal{E}}^{ci})$  as input and generates the probability that the features are from original images. During training, we optimize  $\theta_{\mathcal{J}}$  in an alternating manner along with the compression-insensitive encoder and decoder. The updating of  $\theta_{\mathcal{E}}^{ci}$ ,  $\theta_{\mathcal{D}}^{ci}$  can be formally represented as:

$$\begin{aligned} \theta_{\mathcal{E}}^{ci} &\leftarrow \theta_{\mathcal{E}}^{ci} - lr \nabla_{\theta_{\mathcal{E}}^{ci}} (\mathcal{L}_{cc}^{ci} + \lambda_{ci} \mathcal{L}_{cic}), \\ \theta_{\mathcal{D}}^{ci} &\leftarrow \theta_{\mathcal{D}}^{ci} - lr \nabla_{\theta_{\mathcal{D}}^{ci}} (\mathcal{L}_{cc}^{ci} + \lambda_{ci} \mathcal{L}_{cic}), \end{aligned} \quad (3)$$

and the one of  $\theta_{\mathcal{J}}$ :

$$\theta_{\mathcal{J}} \leftarrow \theta_{\mathcal{J}} - lr \nabla_{\theta_{\mathcal{J}}} (-\mathcal{L}_{cic}), \quad (4)$$

where  $\lambda_{ci}$  is a penalty factor.  $lr$  denotes the learning rate.  $\mathcal{L}_{cc}^{ci}$  and  $\mathcal{L}_{cic}$  denote the content constraint and the compression-insensitive constraint (shown in Fig. 3):

$$\begin{aligned} \mathcal{L}_{cc}^{ci} &= \frac{1}{2N} \sum_{i=1}^N \underbrace{\| \mathcal{D}_{ci}(\mathcal{E}_{ci}(\mathbf{c}_i; \theta_{\mathcal{E}}^{ci}); \theta_{\mathcal{D}}^{ci}) - \mathbf{c}_i \|_1}_{\text{content constraint on } \mathbf{c}_i} \\ &+ \underbrace{\| \mathcal{D}_{ci}(\mathcal{E}_{ci}(\mathbf{o}_i; \theta_{\mathcal{E}}^{ci}); \theta_{\mathcal{D}}^{ci}) - \mathbf{o}_i \|_1}_{\text{content constraint on } \mathbf{o}_i}, \end{aligned} \quad (5)$$

$$\begin{aligned} \mathcal{L}_{cic} &= \frac{1}{2N} \sum_{i=1}^N \underbrace{-\log \mathcal{J}(\mathcal{E}_{ci}(\mathbf{c}_i; \theta_{\mathcal{E}}^{ci}); \theta_{\mathcal{J}})}_{\text{compression-insensitive constraint on } \mathbf{c}_i} \\ &+ \underbrace{\log \mathcal{J}(\mathcal{E}_{ci}(\mathbf{o}_i; \theta_{\mathcal{E}}^{ci}); \theta_{\mathcal{J}})}_{\text{compression-insensitive constraint on } \mathbf{o}_i}. \end{aligned} \quad (6)$$

where  $N$  is the batch size during training. The idea behind this is that it allows one to train an auto-encoder with the goal of fooling a differentiable discriminator network that is trained to distinguish the features of compressed images from that of original images. Fig. 4 exhibits the visualization of the compression-insensitive features learned from two samples.

2) *Compression-Sensitive Auto-Encoder*: As aforementioned, here we resort to the quality factor (QF) to represent the compression degree of compressed images and regularize features to be aware of compression information. Therefore, the features tend to understand low-level details that are sensitive during compression. To this end, we construct an encoder  $\mathcal{E}_{cs}(\cdot; \theta_{\mathcal{E}}^{cs})$  to extract compression-sensitive features and  $\mathcal{D}_{cs}(\cdot; \theta_{\mathcal{D}}^{cs})$  for decoding, which share the same architecture with the compression-insensitive auto-encoder. To extract compression-sensitive features, we rely on an auxiliary compression degree predictor  $\mathcal{P}_{qf}(\cdot; \theta_{\mathcal{P}}^{qf})$  to  $\mathcal{E}_{cs}(\cdot; \theta_{\mathcal{E}}^{cs})$  and  $\mathcal{D}_{cs}(\cdot; \theta_{\mathcal{D}}^{cs})$ . The predictor is a  $2048 \times 2048 \times 100$  MLP, which takes the features extracted by  $\mathcal{E}_{cs}(\cdot; \theta_{\mathcal{E}}^{cs})$  as input and outputs the compression degree. Training an auto-encoder with the goal of predicting the QF from the features could supervise the

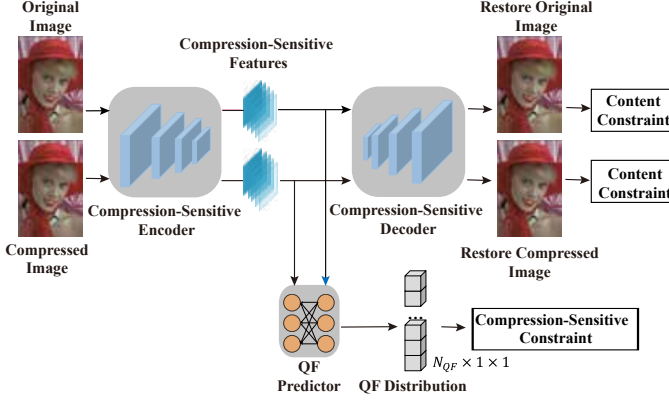


Fig. 5. The training of compression-sensitive auto-encoder. The QF predictor takes the features learned by the compression-sensitive encoder as the input and generates the QF distribution. By training the auto-encoder with the goal of recognizing the QF, we obtain a compression-sensitive encoder that could extract compression-insensitive features from images.

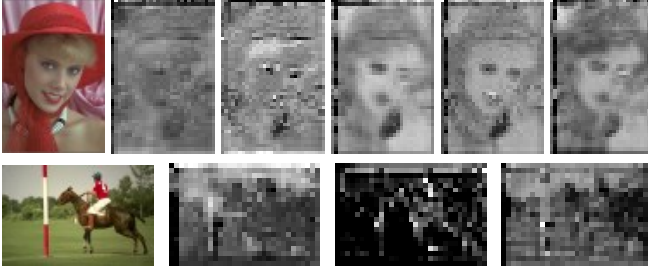


Fig. 6. Visualization of the compression-sensitive features learned from *womanhat* in LIVE1 and *206062* in BSD500.

encoder to extract compression-sensitive features. In training, we update  $\theta_{\mathcal{E}}^{cs}$ ,  $\theta_{\mathcal{D}}^{cs}$ ,  $\theta_{\mathcal{P}}^{qf}$  by:

$$\begin{aligned}\theta_{\mathcal{E}}^{cs} &\leftarrow \theta_{\mathcal{E}}^{cs} - lr \nabla_{\theta_{\mathcal{E}}^{cs}} (\mathcal{L}_{cc}^{cs} + \lambda_{cs} \mathcal{L}_{csc}), \\ \theta_{\mathcal{D}}^{cs} &\leftarrow \theta_{\mathcal{D}}^{cs} - lr \nabla_{\theta_{\mathcal{D}}^{cs}} (\mathcal{L}_{cc}^{cs} + \lambda_{cs} \mathcal{L}_{csc}), \\ \theta_{\mathcal{P}}^{qf} &\leftarrow \theta_{\mathcal{P}}^{qf} - lr \nabla_{\theta_{\mathcal{P}}^{qf}} (\mathcal{L}_{cc}^{cs} + \lambda_{cs} \mathcal{L}_{csc}),\end{aligned}\quad (7)$$

where  $\lambda_{cs}$  is a penalty factor,  $\mathcal{L}_{cc}^{cs}$  and  $\mathcal{L}_{csc}$  denote the content constraint and the compression-sensitive constraint (in Fig. 5):

$$\begin{aligned}\mathcal{L}_{cc}^{cs} &= \frac{1}{2N} \sum_{i=1}^N \underbrace{\|\mathcal{D}_{cs}(\mathcal{E}_{cs}(\mathbf{c}_i; \theta_{\mathcal{E}}^{cs}); \theta_{\mathcal{D}}^{cs}) - \mathbf{c}_i\|_1}_{\text{content constraint on } \mathbf{c}_i} \\ &\quad + \underbrace{\|\mathcal{D}_{cs}(\mathcal{E}_{cs}(\mathbf{o}_i; \theta_{\mathcal{E}}^{cs}); \theta_{\mathcal{D}}^{cs}) - \mathbf{o}_i\|_1}_{\text{content constraint on } \mathbf{o}_i},\end{aligned}\quad (8)$$

$$\begin{aligned}\mathcal{L}_{csc} &= \frac{1}{2N} \sum_{i=1}^N \underbrace{\|\mathcal{P}_{qf}(\mathcal{E}_{cs}(\mathbf{c}_i; \theta_{\mathcal{E}}^{cs}); \theta_{\mathcal{P}}^{qf}) - \text{QF}_c^i\|_1}_{\text{compression-sensitive constraint on } \mathbf{c}_i} \\ &\quad + \underbrace{\|\mathcal{P}_{qf}(\mathcal{E}_{cs}(\mathbf{o}_i; \theta_{\mathcal{E}}^{cs}); \theta_{\mathcal{P}}^{qf}) - \text{QF}_o^i\|_1}_{\text{compression-sensitive constraint on } \mathbf{o}_i},\end{aligned}\quad (9)$$

where QF denotes the one-hot encodings of 100 QF classes. During this standard classification process, the features are aware of the quality factors and thus sensitive to compression

degrees. Fig. 6 visualizes the compression-sensitive features learned from two representative samples.

### B. Dual Awareness Guidance Network

Following the encoding-decoding fashion in compression artifacts reduction [13], [46], [48], [50], [52], our DAGN is also composed of one base encoder and one guided decoder. To build connections and guidance during learning, we introduce three insightful modules, *i.e.*, the compression-insensitive guidance module, compression-sensitive guidance module, and cross-feature fusion module. Fig. 7 shows the whole architecture of DAGN, which takes compression images as input and outputs the artifacts reduction results.

1) *Base Encoder*: The base encoder involves four spatial scales, each of which owns a skip connection to the guided decoder. In each scale, we employ four residual blocks, which are composed of two  $3 \times 3$  convolution layers with ReLU activation and batch normalization in the middle. In the tail of the first three scales, convolutions with  $2 \times 2$  strides are adopted to downscale the features. We set the channel numbers of features in the first to the last scale to 64, 128, 256, and 512, respectively.

2) *Compression-Insensitive Guidance*: The compression-insensitive guidance module aims to extract compression-insensitive features and utilize them to guide the artifacts reduction process. The compression-insensitive guidance takes well-trained insensitive features from the auto-encoder and then learns parameters for transforming feature representations in the decoding process. We employ a three-layer Multi-Layer Perceptron (MLP) as a compression-insensitive guider to learn these transformation features. The first two layers generate shared intermediate conditions, while the last layer generates different parameters  $(\beta_i, \gamma_i)$ ,  $i = 1, 2, 3$  for the three dual awareness guidance blocks in the guided decoder.

3) *Compression-Sensitive Guidance*: Analogous to the insensitive guidance, our goal is to extract compression-sensitive features and utilize them to guide the artifacts reduction process. We first use the compression-sensitive guider to encode compression-insensitive features, then learn parameters  $(\epsilon_i, \eta_i)$ ,  $i = 1, 2, 3$  that could be fused into the dual awareness guidance blocks in the guided decoder.

4) *Cross-Feature Fusion Module*: Compression-insensitive features represent shared semantic information between compressed and original images. This information should be evident in the results of reducing artifacts. To maintain the consistency of compression-insensitive features between original images and artifacts reduction results, we propose the cross-feature fusion module (CFM), which fuses compression-insensitive features into the artifacts reduction baseline.

The compression-insensitive features  $\mathbf{F}_{cif} \in \mathbb{R}^{C_c \times H_c \times W_c}$  and base features  $\mathbf{F}_{bf} \in \mathbb{R}^{C_b \times H_b \times W_b}$  are in different feature spaces. Thus, to fuse them with enhanced receptive fields, CFM firstly conducts three  $1 \times 1$  convolutions to transform  $\mathbf{F}_{cif}$  and  $\mathbf{F}_{bf}$  to features with the same channel number  $C_b$ , where  $\mathcal{C}_1^1(\mathbf{F}_{cif}), \mathcal{C}_2^1(\mathbf{F}_{cif}) \in \mathbb{R}^{C_b \times H_c \times W_c}$ ,  $\mathcal{C}_3^1(\mathbf{F}_{bf}) \in \mathbb{R}^{C_b \times H_b \times W_b}$ , and  $\{\mathcal{C}_i^1(\cdot)\}_{i=1}^3$  denote different  $1 \times 1$  convolutions. Additionally, a pyramid pooling [68] operation  $\text{Pool}$

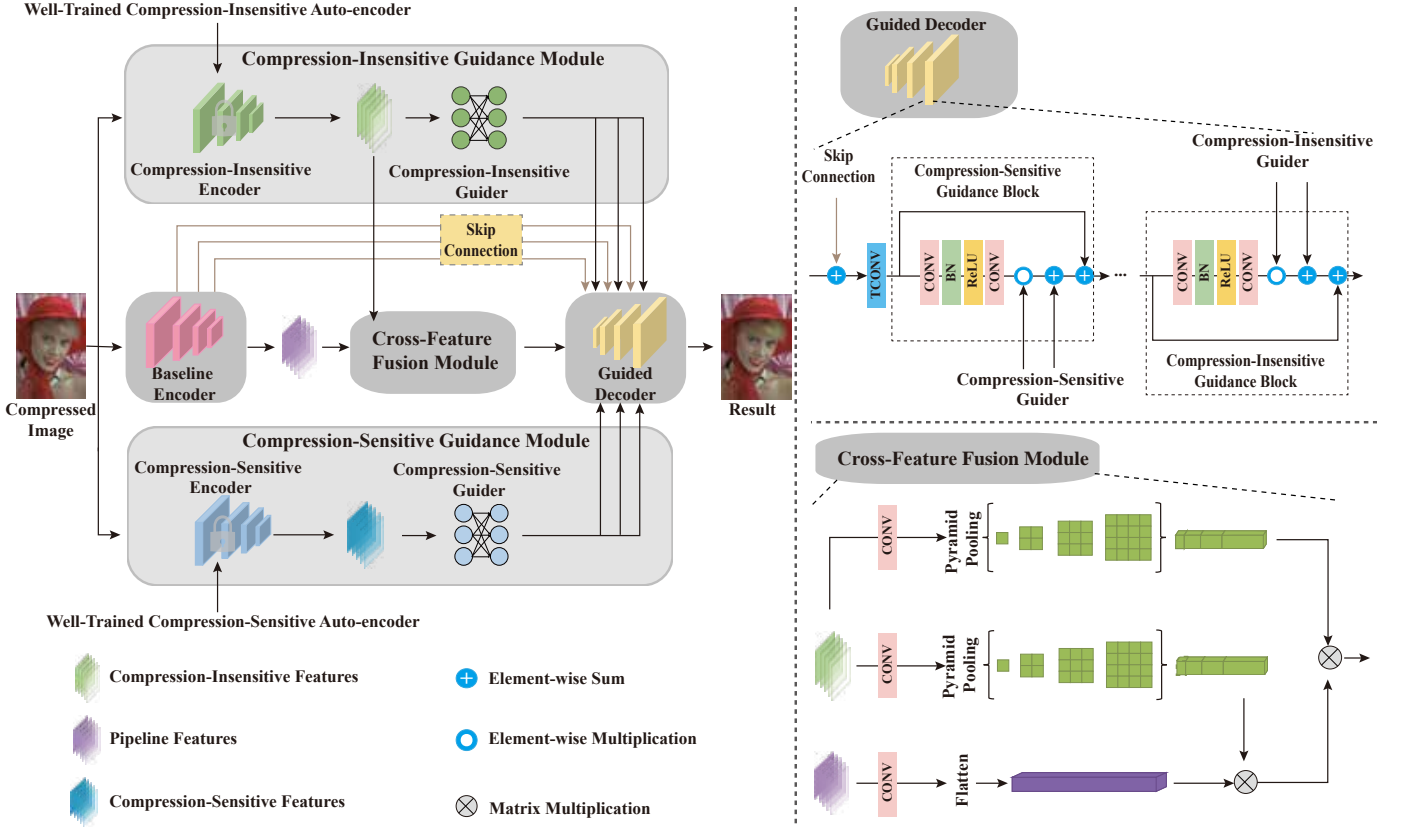


Fig. 7. The architecture of DAGN for compression artifacts reduction. DAGN utilizes the decoupled sensitive and insensitive features as guidance for the feature decoding process. The compression-insensitive guidance module and compression-sensitive guidance module aim to extract compression-insensitive features and compression-sensitive features to guide the compression artifacts reduction process. Cross-feature fusion module aims to fuse compression-insensitive features into the artifacts reduction process.

that contains four pooling layers with different output sizes  $(\{k \times k\}_{k=1,2,4,8})$  in parallel is conducted to sample  $\mathcal{C}_1^1(\mathbf{F}_{cif})$  and  $\mathcal{C}_2^1(\mathbf{F}_{cif})$ . Here  $\text{Pool}(\mathcal{C}_1^1(\mathbf{F}_{cif})), \text{Pool}(\mathcal{C}_2^1(\mathbf{F}_{cif})) \in \mathbb{R}^{C_b \times (\sum_{n=1,2,4,8} n^2)}$ . Our proposed CFM has the following form:

$$\mathcal{M}_{cf}(\mathbf{F}_{cif}, \mathbf{F}_{bf}) = \mathcal{C}_3^1(\mathbf{F}_{bf}) \times \text{Pool}(\mathcal{C}_1^1(\mathbf{F}_{cif})) \times \text{Pool}(\mathcal{C}_2^1(\mathbf{F}_{cif}))^T + \mathbf{F}_{bf}^T, \quad (10)$$

where  $\times$  denotes the matrix multiplication operation, and  $\mathcal{C}_3^1(\mathbf{F}_{bf}) \times \text{Pool}(\mathcal{C}_1^1(\mathbf{F}_{cif}))$  is an approximate similarity matrix between  $\mathbf{F}_{cif}$  and  $\mathbf{F}_{bf}$ .

5) *Guided Decoder Transformation*: The guided decoder transformation aims to utilize the decoupled sensitive and insensitive features as learning guidance to transform the encoded representations, which helps to build an adaptive decoding process under different scenarios. Our guided decoder involves four scales, each of which receives a skip connection to the base encoder. The first scale consists of four residual blocks comprising two  $3 \times 3$  convolution layers with ReLU activation and batch normalization in the middle. The last three scales employ Dual Awareness Guidance Blocks (DAGB). As in Fig. 7, DAGB receives the skip connection from the corresponding scale in the base encoder, and the parameters learned from the compression-sensitive guider and compression-insensitive guider (*i.e.*  $(\beta_i, \gamma_i), (\epsilon_i, \eta_i)$ ). With the embedding dimension of  $D$ , thus  $\beta_i, \gamma_i, \epsilon_i, \eta_i \in \mathbb{R}^{\frac{D}{2^i} \times 1}$

represent the feature scale factors and transformation biases. Specifically, DAGN adopts  $2 \times 2$  transpose convolutions for upscaling operations. Then, four compression-sensitive guidance blocks and four compression-insensitive guidance blocks are utilized to guide the artifacts reduction process by applying transformations to intermediate features.

Let  $\mathbf{F}_{dagb}^{in}$  be the input of one DAGB in the guided decoder, and  $\mathbf{F}_{dagb}^{sc}$  denote the corresponding skip connection. The output of the  $i$ -th DAGB could be written as:

$$\mathcal{B}_{dagb}(\mathbf{F}_{dagb}^{in}, \mathbf{F}_{dagb}^{sc}) = \mathcal{B}_{cig}^4(\mathcal{B}_{csg}^4(\mathcal{T}_2(\mathbf{F}_{dagb}^{in} + \mathbf{F}_{dagb}^{sc}))), \quad (11)$$

where  $\mathcal{T}_2$  denotes the transpose convolution layers;  $\mathcal{B}_{cig}(\cdot)$  and  $\mathcal{B}_{csg}(\cdot)$  denote the compression-insensitive guidance block and compression-sensitive guidance block, respectively.

$$\mathcal{B}_{cig}(\mathbf{F}_{cig}^{in}) = \mathbf{F}_{cig}^{in} + \beta_i \odot \mathcal{C}_1^3(\text{RNORM}(\mathcal{C}_2^3(\mathbf{F}_{cig}^{in}))) + \gamma_i, \quad (12)$$

$$\mathcal{B}_{csg}(\mathbf{F}_{csg}^{in}) = \mathbf{F}_{csg}^{in} + \epsilon_i \odot \mathcal{C}_3^3(\text{RNORM}(\mathcal{C}_4^3(\mathbf{F}_{csg}^{in}))) + \eta_i. \quad (13)$$

Here  $\mathbf{F}_{cig}^{in}$  and  $\mathbf{F}_{csg}^{in}$  denote the input of the compression-insensitive guidance block and the compression-sensitive guidance block, respectively.  $\odot$  is channel-wise multiplication;  $\{\mathcal{C}_i^3(\cdot)\}_{i=1}^4$  are different  $3 \times 3$  convolutions; RNORM denote ReLU activation and batch normalization.

During training, given a batch of training samples, we freeze the parameters of the compression-insensitive encoder and

---

**Algorithm 1** Algorithm of DAGN Training.

```

1: Input: Original and compressed image pairs:  $\mathbb{D} = \langle \mathbf{c}_i, \mathbf{o}_i \rangle$ ,
   hyperparameters  $lr, ite_1, ite_2, \lambda_{ci}, \lambda_{cs}$ .
2: Output: The parameters of DAGN:  $\hat{\theta}_{\mathcal{E}}^{ci}, \hat{\theta}_{\mathcal{E}}^{cs}$ , and  $\hat{\theta}_{res}$ .
   /* Optimization of  $\theta_{\mathcal{E}}^{ci}, \theta_{\mathcal{E}}^{cs}$  */
3:  $ite \leftarrow 0$ 
4: for  $ite < ite_1$  do
5:   Sample a mini-batch  $\langle \mathbf{c}_i, \mathbf{o}_i \rangle \subset \mathbb{D}, i = 1, 2, \dots, N$ 
6:   Calculate  $\mathcal{L}_{cc}^{ci}$  and  $\mathcal{L}_{cic}$  by Equation (5) and (6)
7:   Update  $\theta_{\mathcal{E}}^{ci}, \theta_{\mathcal{D}}^{ci}, \theta_{\mathcal{J}}$  by Equation (3)
8:   Calculate  $\mathcal{L}_{cc}^{cs}$  and  $\mathcal{L}_{csc}$  by Equation (8) and (9)
9:   Update  $\theta_{\mathcal{E}}^{cs}, \theta_{\mathcal{D}}^{cs}, \theta_{\mathcal{P}}^{cf}$  by Equation (7)
10:   $ite \leftarrow ite + 1$ 
11: end for
12:  $\hat{\theta}_{\mathcal{E}}^{ci}, \hat{\theta}_{\mathcal{E}}^{cs} \leftarrow \theta_{\mathcal{E}}^{ci}, \theta_{\mathcal{E}}^{cs}$ 
   /* Optimization of  $\theta_{res}$  */
13:  $ite \leftarrow 0$ 
14: for  $ite < ite_2$  do
15:   Sample a mini-batch  $\langle \mathbf{c}_i, \mathbf{o}_i \rangle \subset \mathbb{D}, i = 1, 2, \dots, N$ 
16:   Calculate  $\mathcal{L}_1$  by Equation (14)
17:   Update  $\theta_{res}$  by Equation (15)
18:    $ite \leftarrow ite + 1$ 
19: end for
20:  $\hat{\theta}_{res} \leftarrow \theta_{res}$ 

```

---

compression-sensitive encoder, and optimize the rest parameters by minimizing the  $\mathcal{L}_1$  pixel loss:

$$\mathcal{L}_1 = \frac{1}{N} \sum_{i=1}^N \left\| \mathcal{F}_{dagn}(\mathbf{c}_i; \hat{\theta}_{\mathcal{E}}^{ci}, \hat{\theta}_{\mathcal{E}}^{cs}, \theta_{res}) - \mathbf{o}_i \right\|_1, \quad (14)$$

$$\theta_{res} \leftarrow \theta_{res} - \nabla_{\theta_{res}} \mathcal{L}_1. \quad (15)$$

Here  $\mathcal{F}_{dagn}(\cdot; \hat{\theta}_{\mathcal{E}}^{ci}, \hat{\theta}_{\mathcal{E}}^{cs}, \theta_{res})$  denotes the DAGN with frozen compression-insensitive encoder and compression-sensitive encoder, where  $\hat{\theta}_{\mathcal{E}}^{ci}$  and  $\hat{\theta}_{\mathcal{E}}^{cs}$  are the parameters of well-trained compression-insensitive encoder and compression-sensitive encoder;  $\theta_{res}$  denotes the rest parameters of DAGN (*i.e.* the parameters of compression-insensitive guider, compression-sensitive guider, base encoder, cross-feature fusion module, and guided decoder). The overall training scheme is summarized in Algorithm 1.

#### IV. EXPERIMENTS

To demonstrate the superiority of DAGN, we conduct quantitative and qualitative evaluations on synthetic JPEG datasets and real-world cases. We compare the proposed DFGN with state-of-the-art methods, including the pioneer DNN-based method ARCNN [41], a dual-domain learning-based method DMCNN [28], two transformer-based methods IPT [45] and SwinIR [46], a quantization table-based method QGAC [61], and a blind method FBCNN [13].

##### A. Experimental Datasets and Setting

1) *Datasets:* Following [13], [61], we employ DIV2K [69] and Flickr2K [70] as training datasets. The former consists of 900 images, and the latter contains 2,650 images. For fair comparisons, the JPEG encoder in MATLAB is employed to compress images used in training and evaluation. Following prevailing methods, we conducted experiments on color JPEG images.

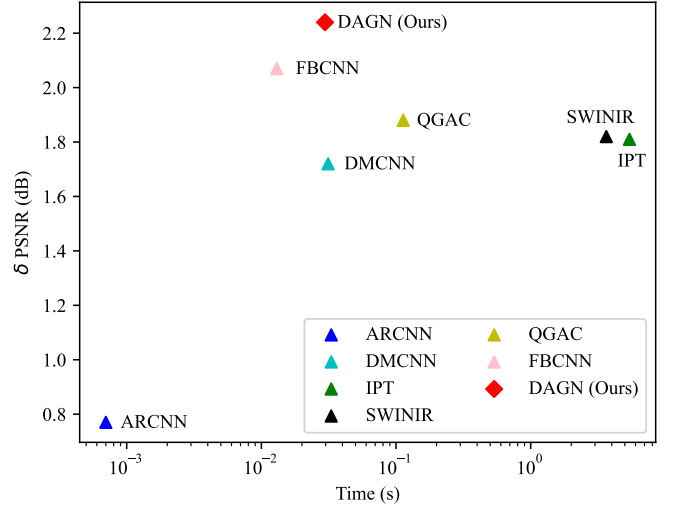


Fig. 8. Average PSNR gains v.s the running times of different methods on the 200 color images with size  $512 \times 512$ .

2) *Training setting of the compression-insensitive encoder and compression-sensitive encoder:* During the compression-insensitive and sensitive encoder training, we randomly sample QF from 10 to 95 to get compressed images. The batch size is set to 32, and each image is resized to  $256 \times 256$ . The optimizer is the Adam [71] with a  $10^{-4}$  learning rate. The learning rate is set to  $5 \times 10^{-4}$  and drops by 0.1 at 5 and 10 epochs. The total epoch is set to 15.

3) *Training setting of DAGN:* We randomly extract a  $96 \times 96$  patch for each training image and compress the patch with QF randomly sampled from 10 to 95. We utilize Adam [71] to optimize the parameters of DAGN by minimizing the  $\mathcal{L}_1$  pixel loss. The batch size is set to 64. The learning rate is set to  $1 \times 10^{-4}$  and decays by a factor of 0.5 at  $8 \times 10^3$  epochs. The total epochs are set to  $1 \times 10^4$ .

##### B. Comparisons with State-of-the-art Methods

1) *Quantitative Comparisons:* We first report the quantitative assessment result of different methods on two widely used datasets, *i.e.*, LIVE1 and BSD500. The peak signal-to-noise ratio (PSNR), structural similarity (SSIM) [76], and peak signal-to-noise ratio including blocking effects (PSNR-B) [77], are conducted for quantitative evaluations. Note that the PSNR-B is specifically designed and more sensitive to blocking artifacts (one of the compression artifacts) than PSNR and SSIM.

Tab. I reports the quantitative results. It is clear that DAGN achieves the best overall result, with significant improvements over other algorithms. For instance, compared with the first deep neural network-based method ARCNN [41], DAGN achieves (1.52 dB, 0.037, and 1.38 dB) improvements in (PSNR, SSIM, and PSNR-B) on LIVE1 and (1.65 dB, 0.022, and 2.00 dB) on BSD500 at QF = 10. Under the same condition, DAGN outperforms the dual-domain learning-based method DMCNN [28] on LIVE1 and BSD500 by (0.77 dB, 0.005, 0.67 dB) and (0.46 dB, 0.003, 0.52 dB), respectively. Compared with the transformer-based method SwinIR [46],

TABLE I  
 QUANTITATIVE COMPARISONS ON LIVE1 AND BSD500. PLEASE NOTE THAT THE MULTI-MODEL METHODS TRAIN A SPECIFIC MODEL FOR EACH QUALITY FACTOR, WHILE THE SINGLE-MODEL METHODS TRAIN ONE MODEL FOR ALL QUALITY FACTORS.

Dataset	QF	Metric	Multi Models				Single Model			
			JPEG	ARCNN [41]	DMCNN [28]	IPT [45]	SWINIR [46]	QGAC [61]	FBCNN [13]	Ours
LIVE1	10	PSNR	25.69	26.43	27.18	27.37	27.45	27.62	<u>27.77</u>	<b>27.95</b>
		SSIM	0.743	0.770	0.802	0.799	0.796	0.804	0.803	<b>0.807</b>
		PSNR-B	24.20	26.32	27.03	27.34	27.23	27.43	<u>27.51</u>	<b>27.70</b>
	20	PSNR	28.06	28.86	30.01	29.99	29.93	29.88	<u>30.11</u>	<b>30.27</b>
		SSIM	0.826	0.843	0.850	0.859	0.866	0.868	<u>0.868</u>	<b>0.873</b>
		PSNR-B	26.49	28.61	29.08	29.51	29.56	29.56	<u>29.70</u>	<b>29.87</b>
	30	PSNR	29.37	29.96	-	31.04	31.12	31.17	<u>31.43</u>	<b>31.60</b>
		SSIM	0.861	0.879	-	0.888	0.896	0.896	<u>0.897</u>	<b>0.900</b>
		PSNR-B	27.84	28.79	-	30.79	30.84	30.77	<u>30.92</u>	<b>31.10</b>
	40	PSNR	30.28	30.78	-	32.09	32.29	32.05	<u>32.34</u>	<b>32.50</b>
		SSIM	0.882	0.896	-	0.903	0.912	0.912	<u>0.913</u>	<b>0.916</b>
		PSNR-B	28.84	29.97	-	31.62	31.78	31.61	<u>31.80</u>	<b>31.94</b>
BSD500	10	PSNR	25.92	26.42	27.61	27.57	27.62	27.74	<u>27.85</u>	<b>28.07</b>
		SSIM	0.739	0.777	0.796	0.792	0.789	<b>0.802</b>	<u>0.799</u>	0.799
		PSNR-B	24.22	25.74	27.22	27.31	27.34	27.47	<u>27.52</u>	<b>27.74</b>
	20	PSNR	28.29	28.84	29.90	29.97	30.03	30.01	<u>30.14</u>	<b>30.36</b>
		SSIM	0.825	0.856	0.863	0.861	0.862	<b>0.869</b>	0.867	0.868
		PSNR-B	26.45	26.48	29.20	29.33	29.51	29.53	<u>29.56</u>	<b>29.77</b>
	30	PSNR	29.64	30.12	-	31.16	31.25	31.33	<u>31.45</u>	<b>31.68</b>
		SSIM	0.863	0.888	-	0.885	0.888	<b>0.898</b>	<u>0.897</u>	<b>0.898</b>
		PSNR-B	27.78	28.20	-	30.74	<u>30.75</u>	30.70	30.72	<b>30.91</b>
	40	PSNR	30.59	30.96	-	32.39	<u>32.44</u>	32.25	32.36	<b>32.58</b>
		SSIM	0.885	0.905	-	0.911	<u>0.913</u>	<b>0.915</b>	0.913	0.914
		PSNR-B	28.74	29.35	-	<u>31.56</u>	31.53	31.5	31.52	<b>31.69</b>

TABLE II  
 QUANTITATIVE COMPARISONS ON LIU4K [40]. PLEASE NOTE THAT THE MULTI-MODEL METHODS TRAIN A SPECIFIC MODEL FOR EACH QUALITY FACTOR, WHILE THE SINGLE-MODEL METHODS TRAIN ONE MODEL FOR ALL QUALITY FACTORS.

Dataset	QF	Metric	Multi Models				Single Model			
			JPEG	ARCNN [41]	DMCNN [28]	IPT [45]	SWINIR [46]	QGAC [61]	FBCNN [13]	Ours
LIU4K	10	PSNR	29.49	30.84	31.76	31.94	31.97	32.10	<u>32.16</u>	<b>32.44</b>
		SSIM	0.809	0.841	0.859	0.861	0.860	<u>0.865</u>	<u>0.865</u>	<b>0.867</b>
		PSNR-B	28.32	30.54	31.65	31.81	31.82	32.04	<u>32.05</u>	<b>32.32</b>
	20	PSNR	32.42	33.20	34.13	34.37	34.40	34.60	<u>34.73</u>	<b>34.94</b>
		SSIM	0.866	0.881	0.895	0.896	0.895	0.900	0.899	<b>0.901</b>
		PSNR-B	31.15	32.97	33.90	34.14	34.14	34.49	<u>34.54</u>	<b>34.69</b>
	30	PSNR	33.87	34.26	-	35.62	35.63	35.85	<u>36.00</u>	<b>36.16</b>
		SSIM	0.892	0.901	-	0.914	0.914	<u>0.917</u>	<u>0.917</u>	<b>0.919</b>
		PSNR-B	32.57	34.07	-	35.32	35.29	35.70	<u>35.75</u>	<b>35.85</b>
	40	PSNR	34.86	34.94	-	36.35	36.40	36.64	<u>36.83</u>	<b>36.96</b>
		SSIM	0.907	0.913	-	0.924	0.924	0.927	<u>0.928</u>	<b>0.929</b>
		PSNR-B	33.54	34.76	-	35.99	36.00	36.46	<u>36.51</u>	<b>36.56</b>

DAGN obtains (0.50 dB, 0.011, 0.47 dB) gains on LIVE1 and (0.45 dB, 0.010, 0.40 dB) on BSD500 at QF = 10, respectively. It should be noted that ARCNN, DMCNN, and SwinIR train one specific network for each QF, while DAGN trains a network for all QFs. Compared with the flexible artifacts reduction method FBCNN [13], which also train a network for all QFs, DAGN obtains (0.16 dB, 0.005, and 0.17 dB) gains in (PSNR, SSIM, and PSNR-B) on LIVE1 and (0.22 dB, 0.001, 0.21 dB) on BSD500 at QF = 20. Similar results could be found at other QFs. These results demonstrate

the superiority of the proposed DAGN over state-of-the-art learning-based methods. Besides, to verify the performance of our method on 4K images, we evaluate DAGN on LIU4K [40], which contains 1500 4K images for training and 80 4K images for validation. Table II shows the results, which also demonstrate the superiority of DAGN.

2) *Qualitative Comparisons*: Besides the quantitative assessment, we present qualitative comparisons. Fig. 9 shows a sample at QF = 10. For comparison, the regions of interest are highlighted. It could be seen that the compression artifacts obviously exist in JPEG images. Although these artifacts could



Fig. 9. Qualitative comparisons on *Womanhat* at  $QF = 10$ . For comparisons, we highlight the regions of interest. Original Image, PSNR | SSIM | PSNR-B. JPEG 27.68 | 0.722 | 26.45. ARCNN [41] 28.36 | 0.753 | 28.34. DMCNN [28] 29.21 | 0.777 | 29.16. IPT [45] 29.36 | 0.778 | 29.32. SwinIR [46] 29.47 | 0.780 | 29.42. QGAC [61] 29.78 | 0.791 | 29.76. FBCNN [13] 29.76 | 0.786 | 29.74. DAGN (ours) 30.03 | 0.793 | 30.03.

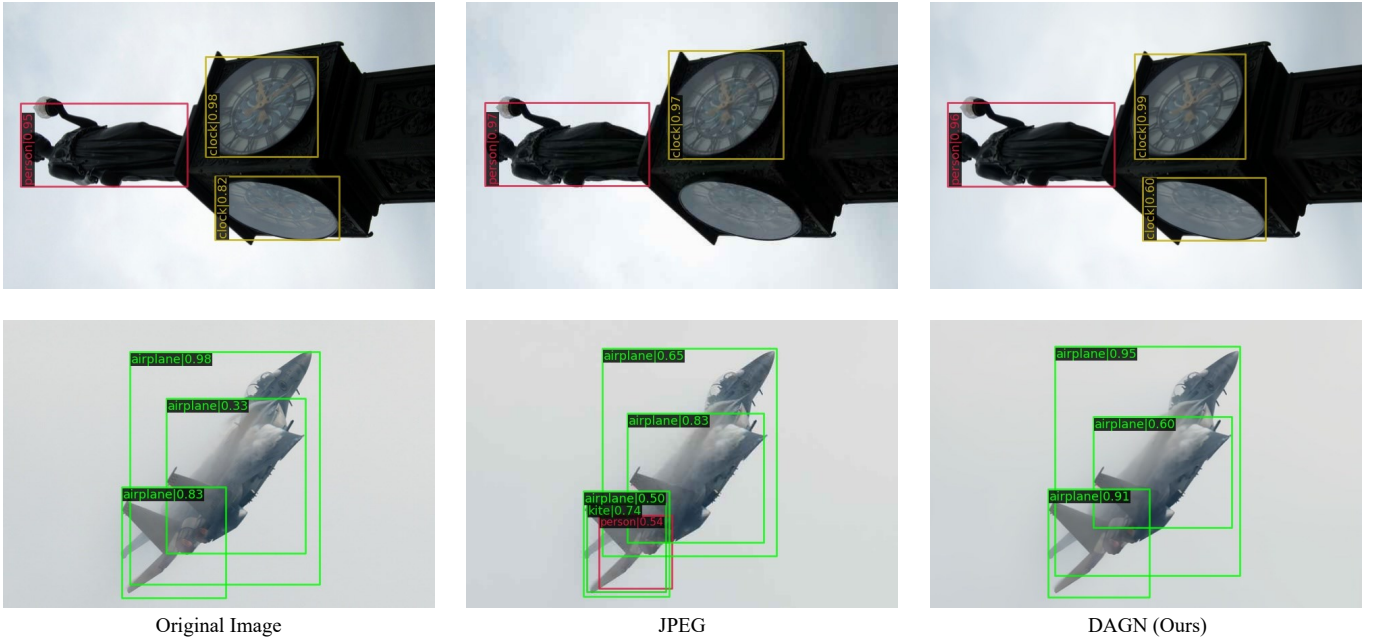


Fig. 10. Object detection results on two samples in MS COCO [72], including the original images + object detection [73], JPEG images ( $QF = 40$ ) + object detection [73], and the compression artifacts results of DAGN + object detection [73].

TABLE III  
FLOPs, THE NUMBER OF PARAMETERS, AND THE RUNNING TIME ON COLOR IMAGES WITH  $512 \times 512$  COLOR IMAGES.

Method	FLOPs (G)	#Params (M)	Running Time (ms)
DMCNN [28]	687.1	4.7	31.3
IPT [45]	70243.5	114.2	5413.7
SWINIR [46]	50768.5	11.5	3643.4
QGAC [61]	249.9	0.0	113.1
FBCNN [13]	728.9	71.9	13.0
Ours	952.8	109.9	29.7

be repressed to different degrees by compression artifacts reduction methods, restoring structures and details is a challenge for the competing methods. By contrast, the proposed

DAGN not only eliminates compression artifacts effectively but also reconstructs more pleasant details and textures than other competing methods.

3) *Efficiency Comparisons*: Table III reports FLOPs, the number of parameters, and the running time of the above methods. Specifically, each method is employed to process  $200 \times 512 \times 512$  color images, and the experiments are conducted on a single NVIDIA Tesla P100-SXM2-16 GB GPU. Moreover, we report the running time and the gains of PSNR in Fig. 8. It could be seen that DAGN outperforms ARCNN by a great margin (over 1.4 dB) at the expense of running time. Compared with DMCNN, QGAC, and FBCNN, whose running times are similar to that of DAGN, it obtains 0.26 dB, 0.25 dB, and 0.19 dB improvements, respectively. Besides, DAGN impressively uses less running time than the transformer-based

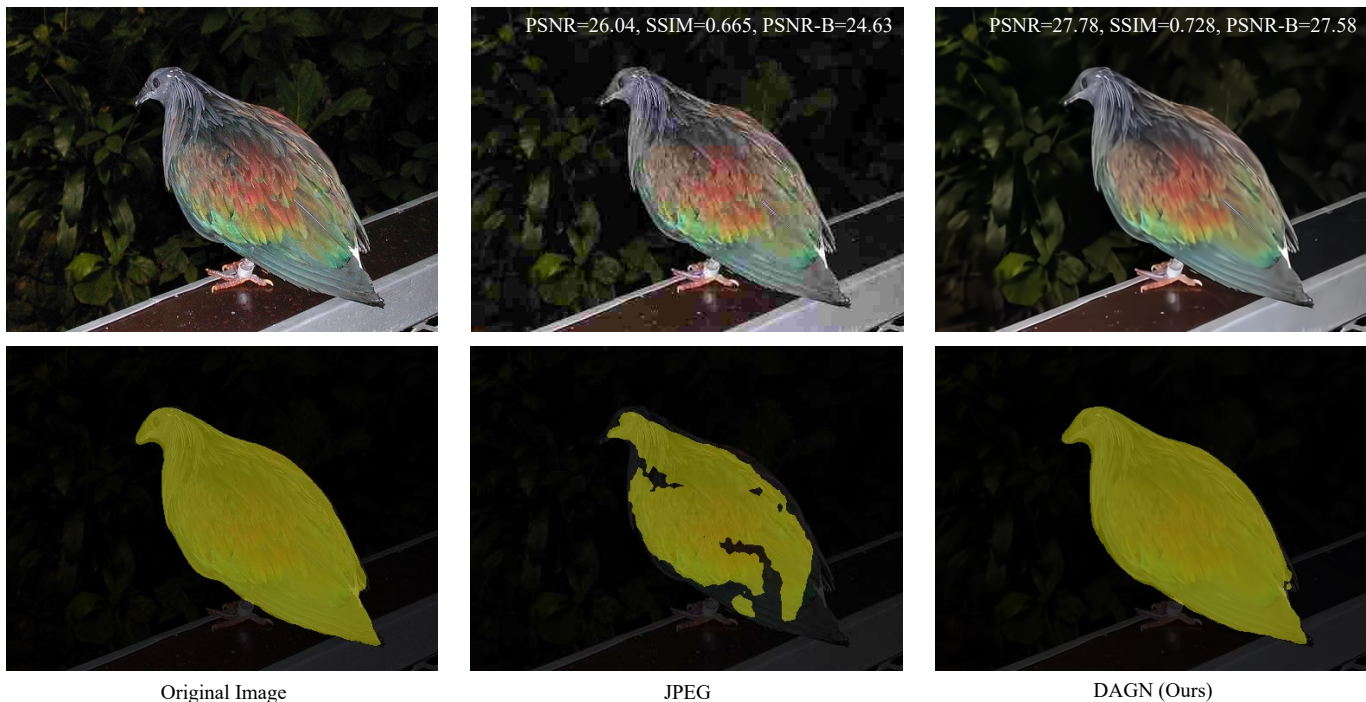


Fig. 11. Comparisons of segmentation results on PASCAL VOC [74]. From left axis to right: the original images + semantic segmentation [75], JPEG images (QF = 10) + semantic segmentation [75], and the compression artifacts results of DAGN + semantic segmentation [75].

TABLE IV

COMPARISONS ON OBJECT DETECTION AND SEMANTIC SEGMENTATION. PLEASE NOTE THAT THE MULTI-MODEL METHODS TRAIN A SPECIFIC MODEL FOR EACH QUALITY FACTOR, WHILE THE SINGLE-MODEL METHODS TRAIN ONE MODEL FOR ALL QUALITY FACTORS.

Task	Metric	QF	Multi-model Methods					Single-model Methods		
			JPEG	ARCNN [41]	DMCNN [28]	IPT [45]	SWINIR [46]	QGAC [61]	FBCNN [13]	Ours
Object detection	Bbox mAP	10	9.5	19.3	22.1	23.7	23.9	<u>24.7</u>	24.5	<b>26.1</b>
		20	23.8	29.1	29.2	29.6	29.8	29.8	<u>30.5</u>	<b>31.6</b>
		30	30.0	31.7	31.9	32.1	32.2	32.0	<u>32.7</u>	<b>33.7</b>
		40	32.2	32.7	32.9	33.1	33.3	33.4	<u>33.4</u>	<b>34.7</b>
Semantic segmentation	mean IoU	10	51.8	55.9	56.2	56.7	56.5	56.8	<u>56.9</u>	<b>57.9</b>
		20	66.9	67.4	67.8	68.2	<u>68.3</u>	68.2	<u>68.3</u>	<b>69.3</b>
		30	71.7	72.3	72.0	72.1	<u>72.5</u>	<u>72.5</u>	72.3	<b>73.1</b>
		40	72.9	73.1	72.8	73.2	73.2	73.3	<u>73.7</u>	<b>74.3</b>

methods, *i.e.*, IPT and SwinIR. It could be observed that our proposed method introduces affordable computation costs but surpasses the prevailing methods by a margin, which indicates that our proposed method achieves a good trade-off considering the performance and time costs.

### C. Evaluations on Computer Vision Tasks

Compression artifacts affect the performance of computer vision tasks apart from decreasing visual quality [40], [43], [78]. In order to reduce the impact of compression artifacts, it may be helpful to suppress them during the preprocessing phase. As a result, we will examine the effectiveness of the proposed DAGN in this subsection, specifically regarding two common computer vision tasks, *i.e.*, object detection, and semantic segmentation.

1) *Object Detection*: The quantitative results are shown in Tab. IV. We could observe that DAGN earns the best

overall result, with significant improvements over the baseline JPEG. Fig. 10 reports the results by Ren *et al.* [73] on original images, JPEG images, and the results of DAGN, respectively. It could be observed that compression artifacts could cause both missing and false detection, and the proposed DAGN could help boost the performance. For example, affected by compression artifacts, one clock is missed in the first axis of Fig. 10, and the airplane is wrongly recognized as a person in the second axis of Fig. 10. In contrast, with the help of DAGN, the detection results are nearly the same as the ones on the original image.

2) *Semantic Segmentation*: The quantitative results are shown in Tab. IV. It could be observed that DAGN earns the best result. The semantic segmentation results by Zhao *et al.* [75] on original images, JPEG images, and the results of DAGN are reported in Fig. 11. One could observe that compression artifacts decrease the visual quality and lead to

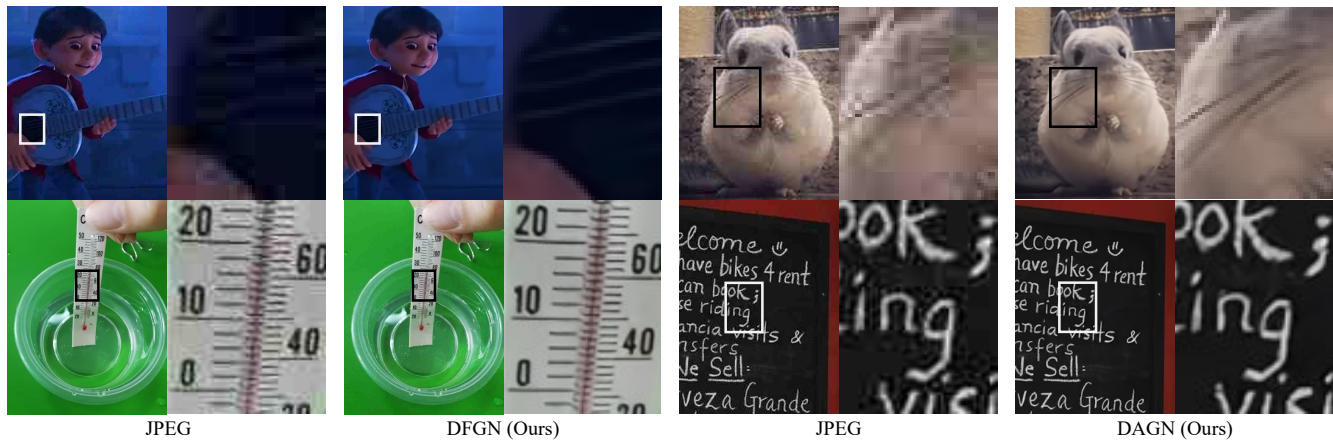


Fig. 12. Comparison before and after applying DAGN on real-world cases. For comparison, the regions of interest are highlighted. It could be observed that DAGN could restore patterns with better visual quality.

TABLE V

QUANTITATIVE COMPARISON WITH DIFFERENT CASES (*i.e.*): BASELINE: ONLY BASE ENCODER AND GUIDED DECODER; BASELINE W. CIGM: BASE ENCODER, GUIDED DECODER, AND COMPRESSION-INSENSITIVE GUIDANCE MODULE; BASELINE W. CSGM: BASE ENCODER, GUIDED DECODER, AND COMPRESSION-SENSITIVE GUIDANCE MODULE; BASELINE W. CFM: BASE ENCODER, GUIDED DECODER, AND CROSS-FEATURE FUSION MODULE. THE BEST SCORES ARE **HIGHLIGHTED**.

Dataset	QF	Metric	Baseline	Baseline w. CIGM	Baseline w. CSGM	Baseline w. CFM	DAGN
LIVE1	10	PSNR	27.46	27.82	27.74	27.72	<b>27.95</b>
		SSIM	0.798	0.803	0.801	0.799	<b>0.807</b>
		PSNR-B	27.11	27.57	27.50	27.47	<b>27.70</b>
	20	PSNR	29.82	30.15	30.08	30.03	<b>30.27</b>
		SSIM	0.866	0.870	0.868	0.866	<b>0.873</b>
		PSNR-B	29.34	29.73	29.68	29.6	<b>29.87</b>
	30	PSNR	31.12	31.47	31.40	31.53	<b>31.60</b>
		SSIM	0.894	0.898	0.897	0.895	<b>0.900</b>
		PSNR-B	30.57	30.95	30.92	30.83	<b>31.10</b>
	40	PSNR	32.01	32.37	32.31	32.20	<b>32.50</b>
		SSIM	0.910	0.914	0.913	0.911	<b>0.916</b>
		PSNR-B	31.44	31.81	31.77	31.64	<b>31.94</b>
BSD500	10	PSNR	27.68	27.96	27.92	27.86	<b>28.07</b>
		SSIM	0.792	0.795	0.793	0.792	<b>0.799</b>
		PSNR-B	27.26	27.64	27.6	27.54	<b>27.74</b>
	20	PSNR	30.00	30.25	30.21	30.13	<b>30.36</b>
		SSIM	0.862	0.865	0.863	0.861	<b>0.868</b>
		PSNR-B	29.36	29.67	29.65	29.54	<b>29.77</b>
	30	PSNR	31.31	31.56	31.52	31.39	<b>31.68</b>
		SSIM	0.893	0.895	0.894	0.891	<b>0.898</b>
		PSNR-B	30.54	30.82	30.81	30.65	<b>30.91</b>
	40	PSNR	32.05	32.47	32.44	32.22	<b>32.58</b>
		SSIM	0.907	0.912	0.911	0.910	<b>0.914</b>
		PSNR-B	31.20	31.61	31.60	31.36	<b>31.69</b>

poor segmentation. Then, we employ the proposed DAGN to mitigate the effect of compression artifacts. It could be seen that the semantic segmentation results from the compression artifacts reduction result produced by DAGN are close to those of the original image. This evidence verifies that our proposed DAGN significantly retains the high-level features for various downstream parsing tasks.

#### D. Real-World Use Cases

Besides the synthetic datasets, we evaluate the proposed DAGN in real-world use cases. Actually, most images shared on the Internet are compressed to save storage space. We collect 100 compressed images from the Internet and apply the proposed DAGN to reduce compression artifacts. Fig. 12 shows four examples. Since there are no original images, the quantitative results are not shown. From Fig. 12, one could observe that there are several artifacts in the online compressed images, degrading the visual experience dramatically. The

proposed DAGN not only significantly represses compression artifacts but also enacts pleasingly on restoring details.

### E. Ablation Study

1) *The contribution of CIGM, SIGM, and CFM*: To further investigate the proposed DAGN, we conduct an ablation study to measure the contribution of the three components, including the compression-insensitive guidance module, compression-sensitive guidance module, and cross-feature fusion module. Tab. V shows the comparisons between models with four different cases:

- **Baseline**: Only the base encoder and guided decoder. Specifically, the guided decoder only takes baseline features as input, and  $(\beta_i, \gamma_i), (\eta_i, \epsilon_i), i = 1, 2, 3$  in the guided decoder are set to  $(\mathbf{O}, \mathbf{J})$  and  $(\mathbf{O}, \mathbf{J})$ , where  $\mathbf{O}$  and  $\mathbf{J}$  indicate zero matrix and all-ones matrix, respectively.
- **Baseline w. CIGM**: The base encoder, the guided decoder, and the compression-insensitive guidance module. Specifically, the guided decoder only takes baseline features as input, and  $(\beta_i, \gamma_i), i = 1, 2, 3$  are generated by the compression-insensitive guider from the compression-insensitive features, while  $(\eta_i, \epsilon_i), i = 1, 2, 3$  in the guided decoder are set to  $(\mathbf{O}, \mathbf{J})$ .
- **Baseline w. CSGM**: The base encoder, the guided decoder, and the compression-sensitive guidance module. Specifically, the guided decoder only takes the baseline features as input, and  $(\eta_i, \epsilon_i), i = 1, 2, 3$  are generated by the compression-sensitive guider from the compression-sensitive features, while  $(\beta_i, \gamma_i), i = 1, 2, 3$  in the guided decoder are set to  $(\mathbf{O}, \mathbf{J})$ .
- **Baseline w. CFM**: The base encoder, the guided decoder, and the cross-feature fusion module. Specifically,  $(\beta_i, \gamma_i), (\eta_i, \epsilon_i), i = 1, 2, 3$  in the guided decoder are set to  $(\mathbf{O}, \mathbf{J})$  and  $(\mathbf{O}, \mathbf{J})$ , respectively.

It could be observed that the artifacts reduction performance has an obvious improvement with the three modules. For example, without the three modules, the baseline model achieves 27.46 dB, 0.798, 27.11 dB on LIVE1 and 27.68 dB, 0.792, 27.26 dB on BSD500 at QF = 10 in (PSNR, SSIM, PSNR-B). Firstly, CIGM considers compression-insensitive features and learns parameters for transforming feature representations in the decoding process. With the guidance of CIGM, the model could improve (0.36 dB, 0.005, 0.46 dB) on LIVE1 and (0.28 dB, 0.003, 0.38 dB) on BSD500. Secondly, when adding the CSGM to the base encoder and guided decoder, the decoding process is adjusted by the parameters learned from compression-sensitive features. With the help of compression-sensitive features that reflect the degree of compression, the artifacts reduction performance is improved from (27.46 dB, 0.798, 27.11 dB) up to (27.74 dB, 0.801, 27.50 dB) on LIVE1 at QF = 10. Thirdly, we fuse compression-insensitive features with baseline features to incorporate the multi-scale semantic information from the compression-insensitive encoders. It could be observed that CFM could improve the artifacts reduction performance from (27.46 dB, 0.798, 27.11 dB) up to (27.72 dB, 0.799, 27.47 dB) on LIVE1 at QF = 10. Finally,

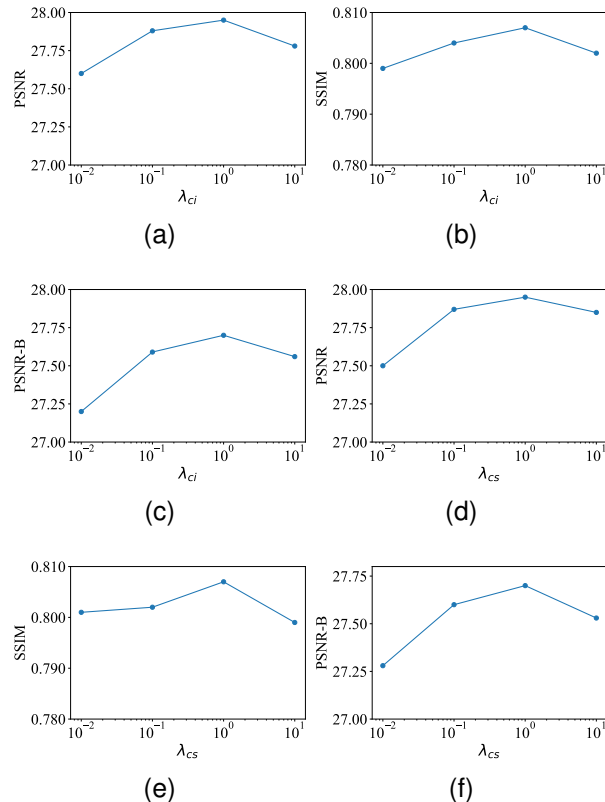


Fig. 13. The performance of DAGNs with different  $\lambda_{ci}$  and  $\lambda_{cs}$

combining the three modules further improves the artifacts reduction performance. These comparisons demonstrate the effectiveness of the compression-insensitive guidance module, compression-sensitive guidance module, and cross-feature fusion module.

2) *The influence of  $\lambda_{ci}$  and  $\lambda_{cs}$* : To explore the impact of  $\lambda_{ci}$  and  $\lambda_{cs}$ , we train DAGNs in the case of  $\lambda_{ci}$  and  $\lambda_{cs}$  with different values. Fig. 13 shows the results. For  $\lambda_{ci}$ , we notice that DAGN achieves the best balance when  $\lambda_{ci} = 1$ , and the model is not very sensitive to  $\lambda_{ci}$ . However, it is essential to avoid using values that are too large or too small since that could decrease the performance of DAGN. This occurs because the compression sensitive encoder focuses on the content-related features and ignores the compression-insensitive features when  $\lambda_{ci} < 1$ . For  $\lambda_{cs}$ , similar conclusions could be drawn from Fig. 13.

## V. CONCLUSION

In this paper, we start from a new view of intrinsic feature decoupling to solve the compression artifacts reduction problem. Toward this end, we propose a dual awareness guidance network for exploiting the intrinsic attributes to guide the learning of artifacts reduction. We first decouple the intrinsic attributes into compression-insensitive features and compression-sensitive features. Then compression-insensitive guidance module, compression-sensitive module, and cross-feature fusion module are designed to employ these features to reduce compression artifacts. Extensive experiments on

synthetic and real compression datasets demonstrate the effectiveness and superiority of the proposed method. One future direction for this work is to explore decoupling learning to other image restoration tasks such as image denoising, super-resolution, and deblurring.

#### ACKNOWLEDGMENT

This work was supported in part by Key-Area Research and Development Program of Guangdong Province under Contract No. 2021B0101400002, and in part by the National Natural Science Foundation of China under Contract No. 62088102, and Contract No. 62202010.

#### REFERENCES

- [1] G. Zhai, W. Zhang, X. Yang, W. Lin, and Y. Xu, "Efficient deblocking with coefficient regularization, shape-adaptive filtering, and quantization constraint," *IEEE Trans. Multimedia*, vol. 10, no. 5, pp. 735–745, 2008.
- [2] S. B. Yoo, K. Choi, and J. B. Ra, "Post-processing for blocking artifact reduction based on inter-block correlation," *IEEE Trans. Multimedia*, vol. 16, no. 6, pp. 1536–1548, 2014.
- [3] A. Foi, V. Katkovnik, and K. Egiazarian, "Pointwise shape-adaptive dct for high-quality denoising and deblocking of grayscale and color images," *IEEE Trans. Image Process.*, vol. 16, no. 5, pp. 1395–1411, 2007.
- [4] J. Zhang, R. Xiong, C. Zhao, Y. Zhang, S. Ma, and W. Gao, "Concolor: Constrained non-convex low-rank model for image deblocking," *IEEE Trans. Image Process.*, vol. 25, no. 3, pp. 1246–1259, 2016.
- [5] X. Liu, X. Wu, J. Zhou, and D. Zhao, "Data-driven soft decoding of compressed images in dual transform-pixel domain," *IEEE Trans. Image Process.*, vol. 25, no. 4, pp. 1649–1659, 2016.
- [6] K. Bredies and M. Holler, "A total variation-based jpeg decompression model," *SIAM Journal on Imaging Sciences*, vol. 5, no. 1, pp. 366–393, 2012.
- [7] H. Chang, M. K. Ng, and T. Zeng, "Reducing artifacts in jpeg decompression via a learned dictionary," *IEEE Trans. Signal Process.*, vol. 62, no. 3, pp. 718–728, 2013.
- [8] Q. Song, R. Xiong, X. Fan, D. Liu, F. Wu, T. Huang, and W. Gao, "Compressed image restoration via artifacts-free pca basis learning and adaptive sparse modeling," *IEEE Trans. Image Process.*, vol. 29, pp. 7399–7413, 2020.
- [9] X. Zhang, W. Lin, R. Xiong, X. Liu, S. Ma, and W. Gao, "Low-rank decomposition-based restoration of compressed images via adaptive noise estimation," *IEEE Trans. Image Process.*, vol. 25, no. 9, pp. 4158–4171, 2016.
- [10] X. Zhang, R. Xiong, X. Fan, S. Ma, and W. Gao, "Compression artifact reduction by overlapped-block transform coefficient estimation with block similarity," *IEEE Trans. Image Process.*, vol. 22, no. 12, pp. 4613–4626, 2013.
- [11] X. Liu, G. Cheung, X. Ji, D. Zhao, and W. Gao, "Graph-based joint dequantization and contrast enhancement of poorly lit jpeg images," *IEEE Trans. Image Process.*, vol. 28, no. 3, pp. 1205–1219, 2018.
- [12] K. Zhang and R. Timofte, "Deep plug-and-play and deep unfolding methods for image restoration," in *Advanced Methods and Deep Learning in Computer Vision*. Elsevier, 2022, pp. 481–509.
- [13] J. Jiang, K. Zhang, and R. Timofte, "Towards flexible blind jpeg artifacts removal," in *Proc. IEEE Int. Conf. Comput. Vis. (ICCV)*, 2021, pp. 4997–5006.
- [14] T. Vandal, E. Kodra, S. Ganguly, A. Michaelis, R. Nemani, and A. R. Ganguly, "Generating high resolution climate change projections through single image super-resolution: An abridged version," in *Proc. Int. Joint Conf. Artif. Intell. (IJCAI)*, 2018.
- [15] Y. Zhang, K. Li, K. Li, B. Zhong, and Y. Fu, "Residual non-local attention networks for image restoration," *arXiv preprint arXiv:1903.10082*, 2019.
- [16] K. Zhang, W. Zuo, Y. Chen, D. Meng, and L. Zhang, "Beyond a gaussian denoiser: Residual learning of deep cnn for image denoising," *IEEE Trans. Image Process.*, vol. 26, no. 7, pp. 3142–3155, 2017.
- [17] K. Li, B. Bare, and B. Yan, "An efficient deep convolutional neural networks model for compressed image deblocking," in *Proc. IEEE Int. Conf. Multimedia Expo (ICME)*. IEEE, 2017, pp. 1320–1325.
- [18] W. Wang, R. Guo, Y. Tian, and W. Yang, "Cfsnet: Toward a controllable feature space for image restoration," in *Proc. IEEE Int. Conf. Comput. Vis. (ICCV)*, 2019, pp. 4140–4149.
- [19] Y. Kim, J. W. Soh, and N. I. Cho, "Agarnet: adaptively gated jpeg compression artifacts removal network for a wide range quality factor," *IEEE Access*, vol. 8, pp. 20 160–20 170, 2020.
- [20] H. Chen, X. He, C. An, and T. Q. Nguyen, "Adaptive image coding efficiency enhancement using deep convolutional neural networks," *Inf. Sci.*, vol. 524, pp. 298–317, 2020.
- [21] Z. Jin, M. Z. Iqbal, W. Zou, X. Li, and E. Steinbach, "Dual-stream multi-path recursive residual network for jpeg image compression artifacts reduction," *IEEE Trans. Circuits Syst. Video Technol.*, vol. 31, no. 2, pp. 467–479, 2020.
- [22] H. Qiu, Q. Zheng, G. Memmi, J. Lu, M. Qiu, and B. Thuraisingham, "Deep residual learning-based enhanced jpeg compression in the internet of things," *IEEE Trans. Ind. Inform.*, vol. 17, no. 3, pp. 2124–2133, 2020.
- [23] Y. Zhang, Y. Tian, Y. Kong, B. Zhong, and Y. Fu, "Residual dense network for image restoration," *IEEE Trans. Pattern Anal. Mach. Intell.*, vol. 43, no. 7, pp. 2480–2495, 2020.
- [24] X. Fu, Z.-J. Zha, F. Wu, X. Ding, and J. Paisley, "Jpeg artifacts reduction via deep convolutional sparse coding," in *Proc. IEEE Conf. Comput. Vis. Pattern Recognit. (CVPR)*, 2019, pp. 2501–2510.
- [25] Z. Wang, D. Liu, S. Chang, Q. Ling, Y. Yang, and T. S. Huang, "D3: Deep dual-domain based fast restoration of jpeg-compressed images," in *Proc. IEEE Conf. Comput. Vis. Pattern Recognit. (CVPR)*, 2016, pp. 2764–2772.
- [26] J. Guo and H. Chao, "Building dual-domain representations for compression artifacts reduction," in *Proc. Eur. Conf. Comput. Vis. (ECCV)*. Springer, 2016, pp. 628–644.
- [27] H. Chen, X. He, L. Qing, S. Xiong, and T. Q. Nguyen, "Dpw-sdnet: Dual pixel-wavelet domain deep cnns for soft decoding of jpeg-compressed images," in *Proc. IEEE Conf. Comput. Vis. Pattern Recognit. Workshop (CVPRW)*, 2018, pp. 711–720.
- [28] X. Zhang, W. Yang, Y. Hu, and J. Liu, "Dmccnn: Dual-domain multi-scale convolutional neural network for compression artifacts removal," in *Proc. IEEE Int. Conf. Image Process. (ICIP)*. IEEE, 2018, pp. 390–394.
- [29] M. Sun, X. He, S. Xiong, C. Ren, and X. Li, "Reduction of jpeg compression artifacts based on dct coefficients prediction," *Neurocomputing*, vol. 384, pp. 335–345, 2020.
- [30] L. Galteri, L. Seidenari, M. Bertini, and A. Del Bimbo, "Deep generative adversarial compression artifact removal," in *Proc. IEEE Conf. Comput. Vis. Pattern Recognit. (CVPR)*, 2017, pp. 4826–4835.
- [31] J. Guo and H. Chao, "One-to-many network for visually pleasing compression artifacts reduction," in *Proc. IEEE Conf. Comput. Vis. Pattern Recognit. (CVPR)*, 2017, pp. 3038–3047.
- [32] L. Galteri, L. Seidenari, M. Bertini, and A. Del Bimbo, "Deep universal generative adversarial compression artifact removal," *IEEE Trans. Multimedia*, vol. 21, no. 8, pp. 2131–2145, 2019.
- [33] H. Chen, X. He, C. An, and T. Q. Nguyen, "Deep wide-activated residual network based joint blocking and color bleeding artifacts reduction for 4: 2: 0 jpeg-compressed images," *IEEE Signal Processing Lett.*, vol. 26, no. 1, pp. 79–83, 2018.
- [34] B. Zheng, Y. Chen, X. Tian, F. Zhou, and X. Liu, "Implicit dual-domain convolutional network for robust color image compression artifact reduction," *IEEE Trans. Circuits Syst. Video Technol.*, vol. 30, no. 11, pp. 3982–3994, 2019.
- [35] J. Li, Y. Wang, H. Xie, and K.-K. Ma, "Learning a single model with a wide range of quality factors for jpeg image artifacts removal," *IEEE Trans. Image Process.*, vol. 29, pp. 8842–8854, 2020.
- [36] Y. Kim, J. W. Soh, J. Park, B. Ahn, H.-S. Lee, Y.-S. Moon, and N. I. Cho, "A pseudo-blind convolutional neural network for the reduction of compression artifacts," *IEEE Trans. Circuits Syst. Video Technol.*, vol. 30, no. 4, pp. 1121–1135, 2019.
- [37] L. Ma, P. Peng, P. Xing, Y. Wang, and Y. Tian, "Reducing image compression artifacts for deep neural networks," in *Proc. Data Compress. Conf. (DCC)*. IEEE, 2021, pp. 355–355.
- [38] L. Ma, Y. Tian, P. Xing, and T. Huang, "Residual-based post-processing for hevc," *IEEE MultiMedia*, vol. 26, no. 4, pp. 67–79, 2019.
- [39] T. Wang, M. Chen, and H. Chao, "A novel deep learning-based method of improving coding efficiency from the decoder-end for hevc," in *Proc. Data Compress. Conf. (DCC)*. IEEE, 2017, pp. 410–419.
- [40] J. Liu, D. Liu, W. Yang, S. Xia, X. Zhang, and Y. Dai, "A comprehensive benchmark for single image compression artifact reduction," *IEEE Trans. Image Process.*, vol. 29, pp. 7845–7860, 2020.

- [41] C. Dong, Y. Deng, C. Change Loy, and X. Tang, "Compression artifacts reduction by a deep convolutional network," in *Proc. IEEE Int. Conf. Comput. Vis. (ICCV)*, 2015, pp. 576–584.
- [42] J. Mu, R. Xiong, X. Fan, D. Liu, F. Wu, and W. Gao, "Graph-based non-convex low-rank regularization for image compression artifact reduction," *IEEE Trans. Image Process.*, vol. 29, pp. 5374–5385, 2020.
- [43] H. Chen, X. He, H. Yang, L. Qing, and Q. Teng, "A feature-enriched deep convolutional neural network for jpeg image compression artifacts reduction and its applications," *IEEE Trans. Neural Netw. Learn. Syst.*, vol. 33, no. 1, pp. 430–444, 2021.
- [44] Z. Zha, B. Wen, X. Yuan, J. T. Zhou, J. Zhou, and C. Zhu, "Triply complementary priors for image restoration," *IEEE Trans. Image Process.*, vol. 30, pp. 5819–5834, 2021.
- [45] H. Chen, Y. Wang, T. Guo, C. Xu, Y. Deng, Z. Liu, S. Ma, C. Xu, C. Xu, and W. Gao, "Pre-trained image processing transformer," in *Proc. IEEE Conf. Comput. Vis. Pattern Recognit. (CVPR)*, 2021, pp. 12 299–12 310.
- [46] J. Liang, J. Cao, G. Sun, K. Zhang, L. Van Gool, and R. Timofte, "Swinir: Image restoration using swin transformer," in *Proc. IEEE Int. Conf. Comput. Vis. (ICCV)*, 2021, pp. 1833–1844.
- [47] J. Cao, Y. Li, K. Zhang, and L. Van Gool, "Video super-resolution transformer," *arXiv preprint arXiv:2106.06847*, 2021.
- [48] Z. Wang, X. Cun, J. Bao, and J. Liu, "Uformer: A general u-shaped transformer for image restoration," *arXiv preprint arXiv:2106.03106*, 2021.
- [49] K. Zhang, W. Zuo, and L. Zhang, "Deep plug-and-play super-resolution for arbitrary blur kernels," in *Proc. IEEE Conf. Comput. Vis. Pattern Recognit. (CVPR)*, 2019, pp. 1671–1681.
- [50] W. Dong, P. Wang, W. Yin, G. Shi, F. Wu, and X. Lu, "Denoising prior driven deep neural network for image restoration," *IEEE Trans. Pattern Anal. Mach. Intell.*, vol. 41, no. 10, pp. 2305–2318, 2018.
- [51] Y. Jo, S. Y. Chun, and J. Choi, "Rethinking deep image prior for denoising," in *Proc. IEEE Int. Conf. Comput. Vis. (ICCV)*, 2021, pp. 5087–5096.
- [52] K. Zhang, Y. Li, W. Zuo, L. Zhang, L. Van Gool, and R. Timofte, "Plug-and-play image restoration with deep denoiser prior," *IEEE Trans. Pattern Anal. Mach. Intell.*, 2021.
- [53] X. Fu, X. Wang, A. Liu, J. Han, and Z.-J. Zha, "Learning dual priors for jpeg compression artifacts removal," in *Proc. IEEE Int. Conf. Comput. Vis. (ICCV)*, 2021, pp. 4086–4095.
- [54] X. Fu, M. Wang, X. Cao, X. Ding, and Z.-J. Zha, "A model-driven deep unfolding method for jpeg artifacts removal," *IEEE Trans. Neural Netw. Learn. Syst.*, 2021.
- [55] R. Liu, L. Ma, Y. Zhang, X. Fan, and Z. Luo, "Underexposed image correction via hybrid priors navigated deep propagation," *IEEE Trans. Neural Netw. Learn. Syst.*, 2021.
- [56] K. Zhang, W. Zuo, S. Gu, and L. Zhang, "Learning deep cnn denoiser prior for image restoration," in *Proc. IEEE Conf. Comput. Vis. Pattern Recognit. (CVPR)*, 2017, pp. 3929–3938.
- [57] R. Liu, Z. Jiang, X. Fan, and Z. Luo, "Knowledge-driven deep unrolling for robust image layer separation," *IEEE Trans. Neural Netw. Learn. Syst.*, vol. 31, no. 5, pp. 1653–1666, 2019.
- [58] K. He, X. Zhang, S. Ren, and J. Sun, "Deep residual learning for image recognition," in *Proc. IEEE Conf. Comput. Vis. Pattern Recognit. (CVPR)*, 2016.
- [59] A. Vaswani, N. Shazeer, N. Parmar, J. Uszkoreit, L. Jones, A. N. Gomez, L. Kaiser, and I. Polosukhin, "Attention is all you need," in *Proc. Adv. Neural Inf. Process. Syst. (NeurIPS)*, 2017, pp. 5998–6008.
- [60] A. Radford, L. Metz, and S. Chintala, "Unsupervised representation learning with deep convolutional generative adversarial networks," *arXiv preprint arXiv:1511.06434*, 2015.
- [61] M. Ehrlich, L. Davis, S.-N. Lim, and A. Shrivastava, "Quantization guided jpeg artifact correction," in *Proc. Eur. Conf. Comput. Vis. (ECCV)*. Springer, 2020, pp. 293–309.
- [62] P. Liu, H. Zhang, K. Zhang, L. Lin, and W. Zuo, "Multi-level wavelet-cnn for image restoration," in *Proc. IEEE Conf. Comput. Vis. Pattern Recognit. Workshop (CVPRW)*, 2018, pp. 773–782.
- [63] Y. Bengio *et al.*, "Learning deep architectures for ai," *Found. Trends Mach. Learn.*, vol. 2, no. 1, pp. 1–127, 2009.
- [64] A. Ng *et al.*, "Sparse autoencoder," *CS294A Lecture notes*, vol. 72, no. 2011, pp. 1–19, 2011.
- [65] C.-Y. Liou, W.-C. Cheng, J.-W. Liou, and D.-R. Liou, "Autoencoder for words," *Neurocomputing*, vol. 139, pp. 84–96, 2014.
- [66] Q. Meng, D. Catchpole, D. Skillicorn, and P. J. Kennedy, "Relational autoencoder for feature extraction," in *Proc. IEEE Int. Joint Conf. Neural Netw. (IJCNN)*. IEEE, 2017, pp. 364–371.
- [67] M. Tschannen, O. Bachem, and M. Lucic, "Recent advances in autoencoder-based representation learning," *arXiv preprint arXiv:1812.05069*, 2018.
- [68] S. Lazebnik, C. Schmid, and J. Ponce, "Beyond bags of features: Spatial pyramid matching for recognizing natural scene categories," in *Proc. IEEE Conf. Comput. Vis. Pattern Recognit. (CVPR)*, vol. 2, 2006, pp. 2169–2178.
- [69] E. Agustsson and R. Timofte, "Ntire 2017 challenge on single image super-resolution: Dataset and study," in *Proc. IEEE Conf. Comput. Vis. Pattern Recognit. Workshops (CVPRW)*, 2017, pp. 1122–1131.
- [70] R. e. Timofte, "Ntire 2017 challenge on single image super-resolution: Methods and results," in *Proc. IEEE Conf. Comput. Vis. Pattern Recognit. Workshops (CVPRW)*, 2017, pp. 1110–1121.
- [71] D. P. Kingma and J. Ba, "Adam: A method for stochastic optimization," in *Proc. Int. Conf. Learn. Represent. (ICLR)*, 2015.
- [72] T. Y. Lin, M. Maire, S. Belongie, L. Bourdev, R. Girshick, J. Hays, P. Perona, D. Ramanan, C. L. Zitnick, and P. Dollár, "Microsoft coco: Common objects in context," in *Proc. IEEE Conf. Comput. Vis. Pattern Recognit. (CVPR)*, 2014.
- [73] S. Ren, K. He, R. Girshick, and J. Sun, "Faster r-cnn: Towards real-time object detection with region proposal networks," *IEEE Trans. Pattern Anal. Mach. Intell.*, Jun 2017.
- [74] M. Everingham, L. Van Gool, C. K. Williams, J. Winn, and A. Zisserman, "The pascal visual object classes (voc) challenge," *Int. J. Comput. Vis.*, vol. 88, no. 2, pp. 303–338, 2010.
- [75] H. Zhao, J. Shi, X. Qi, X. Wang, and J. Jia, "Pyramid scene parsing network," in *Proc. IEEE Conf. Comput. Vis. Pattern Recognit. (CVPR)*, 2017.
- [76] Z. Wang, A. Bovik, H. Sheikh, and E. Simoncelli, "Image quality assessment: from error visibility to structural similarity," *IEEE Trans. Image Process.*, vol. 13, no. 4, pp. 600–612, 2004.
- [77] C. Yim and A. C. Bovik, "Quality assessment of deblocked images," *IEEE Trans. Image Process.*, vol. 20, no. 1, pp. 88–98, 2011.
- [78] W. Gao, S. Ma, L. Duan, Y. Tian, P. Xing, Y. Wang, S. Wang, H. Jia, and T. Huang, "Digital retina: A way to make the city brain more efficient by visual coding," *IEEE Trans. Circuits Syst. Video Technol.*, vol. 31, no. 11, pp. 4147–4161, 2021.

**Li Ma** received the B.S. degree from School of Mathematical Sciences and the Ph.D. degree from School of Computer Sciences, Peking University, Beijing, China, in 2016 and 2023. He joined Huawei Technologies Company, Ltd. in 2023. His research interests include video coding, video generation, and image/video understanding.



**Yifan Zhao** (Member, IEEE) is currently an Associated Professor with the School of Computer Science and Engineering, Beihang University, Beijing, China. He worked as a Boya Postdoc researcher with the School of Computer Science, Peking University. He received the B.E. degree from the Harbin Institute of Technology in Jul. 2016 and the Ph.D. degree from the School of Computer Science and Engineering, Beihang University, in Oct. 2021. His research interests include computer vision, VR/AR, and image/video understanding.



**Peixi Peng** received the PhD degree from Peking University, in 2017, Beijing, China. He is currently an associate researcher with the School of Computer Science, Peking University, Beijing, China, and is also the assistant researcher of Artificial Intelligence Research Center, Peng Cheng Laboratory, Shenzhen, China. He is the author or co-author of more than 20 technical articles in refereed journals such as IEEE TPAMI, PR and conferences such as CVPR/ECCV/IJCAI/ACMMM/AAAI. His research interests include computer vision, multimedia big data, and reinforcement learning.



data, and reinforcement learning.



**Yonghong Tian** (S'00-M'06-SM'10-F'22) is currently the Dean of School of Electronics and Computer Engineering, a Boya Distinguished Professor with the School of Computer Science, Peking University, China, and is also the deputy director of Artificial Intelligence Research, PengCheng Laboratory, Shenzhen, China. His research interests include neuromorphic vision, distributed machine learning and AI for Science. He is the author or coauthor of over 350 technical articles in refereed journals and conferences. Prof. Tian was/is an Associate

Editor of IEEE TCSVT (2018.1-2021.12), IEEE TMM (2014.8-2018.8), IEEE Multimedia Mag. (2018.1-2022.8), and IEEE Access (2017.1-2021.12). He co-initiated IEEE Int'l Conf. on Multimedia Big Data (BigMM) and served as the TPC Co-chair of BigMM 2015, and also served as the Technical Program Co-chair of IEEE ICME 2015, IEEE ISM 2015 and IEEE MIPR 2018/2019, and General Co-chair of IEEE MIPR 2020 and ICME2021. He is a TPC Member of more than ten conferences such as CVPR, ICCV, ACM KDD, AAAI, ACM MM and ECCV. He was the recipient of the Chinese National Science Foundation for Distinguished Young Scholars in 2018, two National Science and Technology Awards and three ministerial-level awards in China, and obtained the 2015 EURASIP Best Paper Award for Journal on Image and Video Processing, and the best paper award of IEEE BigMM 2018, and the 2022 IEEE SA Standards Medallion and SA Emerging Technology Award. He is a Fellow of IEEE, a senior member of CIE and CCF, a member of ACM.